Thermal Analysis of an Electrical Traction Motor with an Air Cooled Rotor

Markus Jaeger, Andreas Ruf and Kay Hameyer
Institute for Electrical Machines (IEM)
RWTH Aachen University
Aachen, Germany
Email: Markus.Jaeger@iem.rwth-aachen.de
Telephone: +49 241 80 97680

Thorben Grosse-von Tongeln
Siemens Mobile Divison, Mainline Transport
Siemens AG
Krefeld, Germany
Email: Thorben.Grosse@siemens.com
Telephone: +49 2151 450-1330

***Abstract*—At low vehicle speed typical for urban areas the thermal limits of the electrical machine are mostly not reached due to the thermal time constants being much higher than the short time spans of high power demand. However in a highway scenario a higher power is required continuously. Due to rotor iron losses caused by the high frequency of the modern traction drive and the thermally insulating air gap at high speeds the rotor is the crucial element in terms of temperature. In this paper the effect of an interior rotor air cooling to improve the thermal utilization is studied.**

***Index Terms*—Electric Vehicles, Traction Drives, Rotating Electrical Machines, Permanent Magnet Synchronous Machines, Thermal Management, Rotor Air Cooling**

I. Introduction

Various studies on the thermal behavior and overload capability of electrical machines can be found in literature [1] [2]. In [3] a convection cooled machine is investigated, intended for use in an range extender module with a rated speed of $2750\,\mathrm{min}^{-1}$. This is much lower than modern traction drives featuring a speed in the range of $11\,300\,\mathrm{min}^{-1}$ (Renault Zoe), $11\,400\,\mathrm{min}^{-1}$ (BMW i3, Nissan Leaf) or $12\,000\,\mathrm{min}^{-1}$ (Tesla Model S, Smart Electric Drive). In [4] the thermal behavior of a traction drive with a rated power of $46\,\mathrm{kW}$ and a maximum speed of $6000\,\mathrm{min}^{-1}$ is analyzed. However studies of the thermal behavior of the rotor of radial field machines which consider high machine speed are rare, despite the rotor being the limiting factor for power output at this speed. To improve the thermal utilization of the electrical machine the effect of an integrated rotor air cooling system is analyzed and the possible load determined.

II. Approach

To determine the possible load the machine temperatures are calculated and compared to the permitted temperatures. Therefor a lumped parameter thermal model (LPTN) is established. Model parameters with significant uncertainties, in particular the convection coefficients and thermal properties of the winding and grouting, are estimated with an optimization algorithm on a series of eight different measurements. As starting point for the convection coefficients analytical and empirical approaches from [5] [6] are used. The distribution of the iron losses is calculated using finite element analysis (FEA) in combination with the iron loss formula from [7]. The material iron loss parameters from that paper were fitted to a measured map of the total iron losses of the machine. For more details about thermal simulation see for example [8].

The insulation system of the winding is classified for $180\,°\mathrm{C}$ (DIN EN 60085 [10]). High temperatures lead to accelerated aging and reduced life time, therefor this limit is used. With a method for calculating the aging effects higher short time temperature limits could be allowed. The permitted permanent magnet temperature depends on the counter acting magnetic field, therefore at low magnet temperatures a higher load can be tolerated. In contrast to the winding exceeding the temperature limit leads to irreversible demagnetization. Using FEA and the permanent magnet characteristic an allowed temperature for every operating point is determined. Since the permanent magnet characteristic is not ideal linear, a small demagnetization of $0.1\,\%$ is allowed.

III. Permanent Magnet Synchronous Machine with Air Cooled Rotor

The studied machine is an radial flux PMSM with internal magnets. Main machine parameters are collected in table I. The rotor air cooling system is constructed internally inside the shaft, with air intake and output on the same side. In the harsh environment of a vehicle the air can be loaded with water, salt or other aggressive substances. The advantage of this concept is a separation of the air flow from the sensitive active components. Therefor a less complex air filter system is sufficient.

The hollow shaft features aluminum cooling fins on the inside. Through the rotation of the fins and the static guidance

TABLE I
Main machine parameters

Rated power	$30\,\mathrm{kW}$	Yoke outer diameter	$202\,\mathrm{mm}$
Rated torque	$100\,\mathrm{Nm}$	Air gap diameter	$122\,\mathrm{mm}$
Max. speed	$10\,000\,\mathrm{min}^{-1}$	Shaft inner diameter	$82\,\mathrm{mm}$
Pole pairs	3	Active length	$80\,\mathrm{mm}$
Slots	36		

978-1-5386-3048-8/18/$31.00 ©2018 IEEE

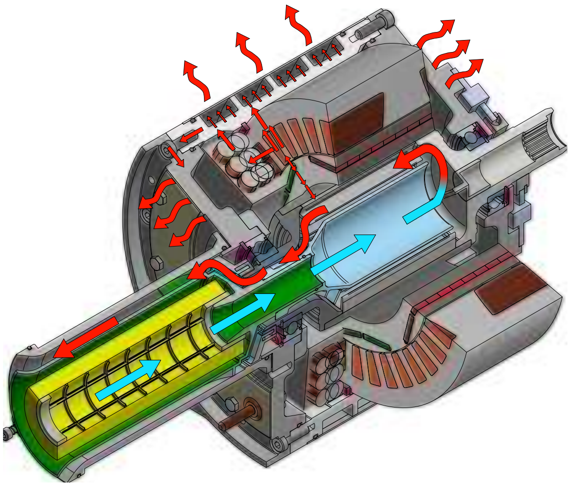

Fig. 1. Machine design with rotor air cooling system.

plates of the tube inside the shaft a speed dependent air flow is achieved. In addition to the cooling of the electrical machine the air flow is used to cool the inverter system, which is mounted circularly around the intake/output tube. The system is illustrated in Fig. 1, the inverter itself is not shown. Further information on the machine can be found in [9].

IV. Thermal Model

A rotational electrical machine features a good radial symmetry to the rotational axis, and to some degree a symmetry to the axial center plane depending on the endwindings, shaft and endshield with bearings. In this paper it is taken advantage of these symmetries for simplification of the model structure. The LPTN is shown in fig. 3, and a sketch to illustrate the areas/volumes represented by the distinct nodes is given in fig. 2.

The heat path in radial direction is represented in fig. 3 by the resistances and thermal masses in vertical direction. For the axial direction it is assumed that in the stacked sheet metal the heat flow is zero. This assumption is feasible due to two reasons: 1. The thermally insulating varnish layers reduce the thermal conductivity of the iron core, and 2. the heat is primarily dissipated through the water cooling jacket and the rotor cooling, therefor in axial direction the temperature gradient is low.

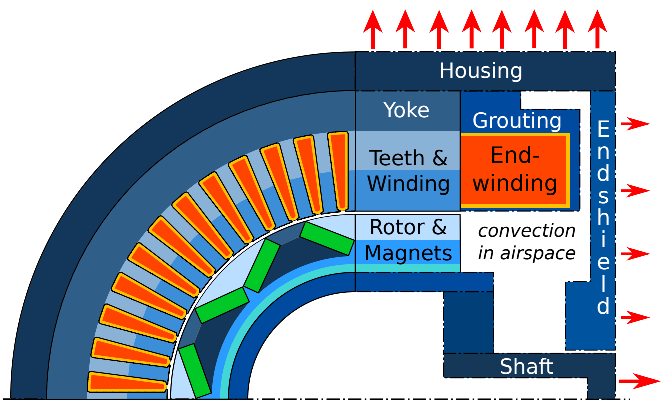

Fig. 2. Sketch of cross section and longitudinal section of the Machine to illustrate the structure of the thermal model.

Table II lists some thermal conductivities and convection coefficients which where in combination with the machine dimensions used to calculate the thermal resistances. The rotor cooling was modeled with the MATLAB/Simscape thermal fluid box and the parameters again fitted with measurements, so no simple convection coefficient can be given.

In fig. 4 the fitted convection coefficient for the airgap is shown which is implemented as a saturation formula based on the approach in [6].

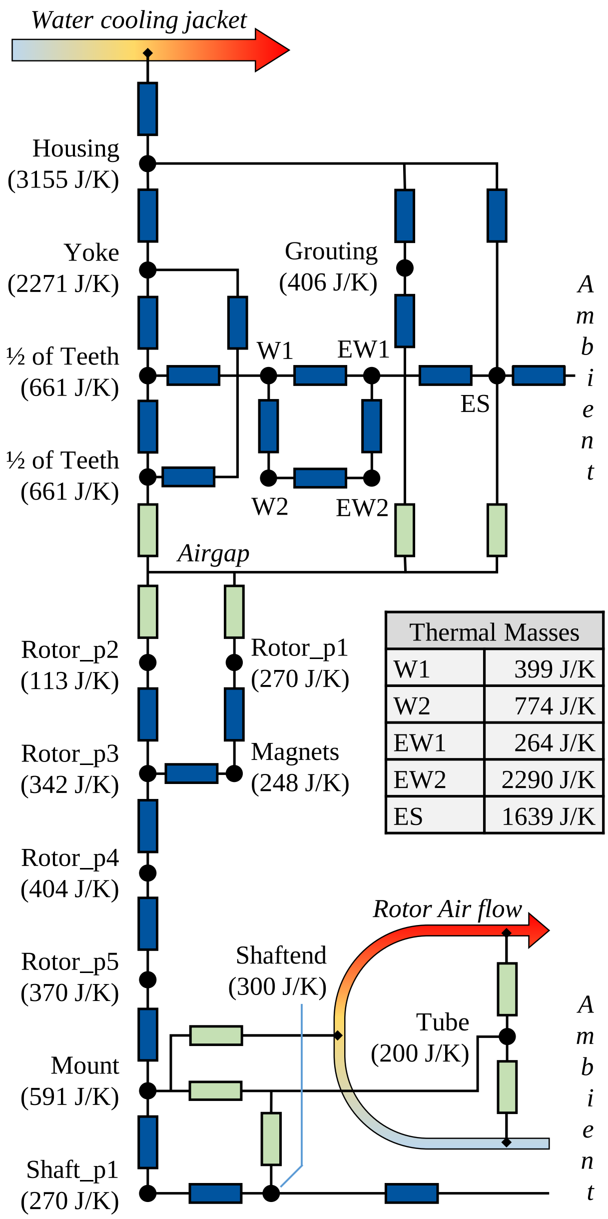

Fig. 3. Schematic diagram of the LPTN considered. Black nodes are thermal capacitors, light green resistances indicate a variable resistance representing machine speed dependent convection.

TABLE II
MAIN MACHINE PARAMETERS

	Thermal conductivity or convection coefficient
Water Jacket	$503\,\mathrm{W/m^2\,K}$ (full Housing cylinder)
Sheet Metal	$23\,\mathrm{W/mK}$ (in sheet plane)
Winding	$174\,\mathrm{W/mK}$ (axial direction)
	$12\,\mathrm{W/mK}$ (radial direction)
Grouting	$1\,\mathrm{W/mK}$

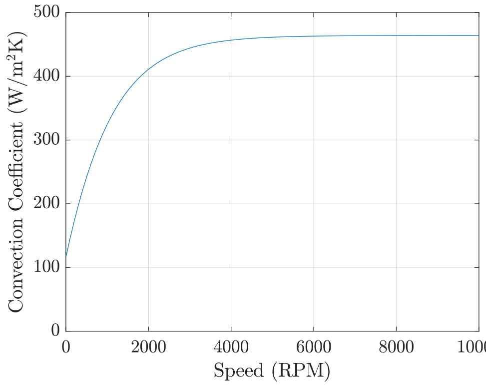

Fig. 4. Fitted convection coefficient in airgap over machine speed.

V. Validation of the Thermal Model

Measured and simulated temperatures for four measurement series are given in Fig. 5-8. The measured temperatures are from six sensors in the end winding on one axial machine end, two sensors in magnet recesses and one sensor between the shaft and the rotor core.

The measured temperatures at the six end winding sensors show consistent differences of up to 20 K which indicates a dependency of the local positioning of the sensor. Insulation aging and possible failure will occur primarily at the end winding hot spots, therefor the measurement data from the hotter three sensors is used for parameter identification of the thermal model.

The model with identified parameters shows good accordance to the measurements with deviations lower than the local temperature differences. The accordance also applies for different operating points with different loss-distributions, different coolant temperatures, with or without rotor cooling. The impact of the iron loss distribution can be observed in Fig. 7. At the time instant of "minute 27" the model shows slightly lower temperatures than measured. A decrease of load does not change the thermal properties which are constant or speed dependent (convection), but leads to slightly higher temperatures in comparison to the measurement at "minute 47". This leads to the conclusion of deviations in the iron loss calculation from the real iron loss distribution.

VI. Effect of the Rotor Air Cooling System

The rotor cooling yields a significant temperature decrease of the magnets depending on the operating point. Because of the speed dependent flow rate the biggest temperature decrease

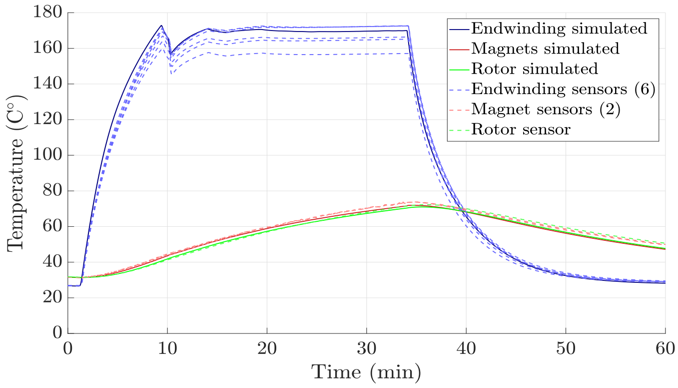

Fig. 5. High load at $50\,\mathrm{min^{-1}}$ with high copper losses. Water coolant intake at $20\,°\mathrm{C}$, rotor cooling active.

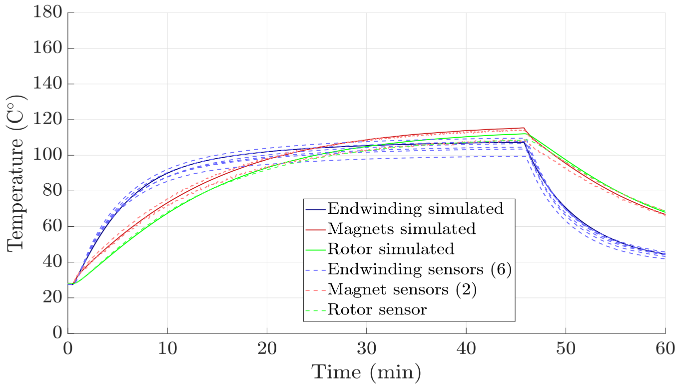

Fig. 6. High load at $9500\,\mathrm{min^{-1}}$ with high iron losses. Water coolant intake at $80\,°\mathrm{C}$, rotor cooling not active.

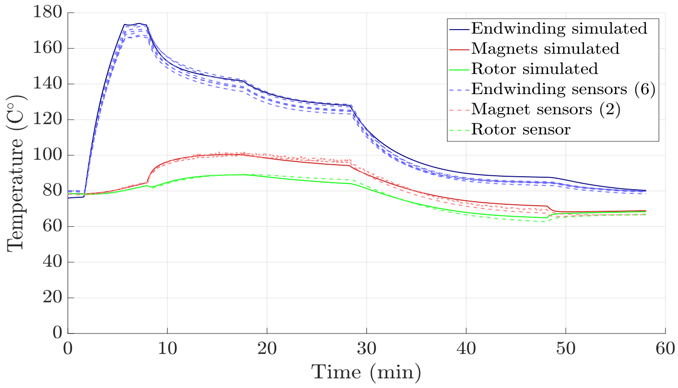

Fig. 7. High load at $50\,\mathrm{min^{-1}}$, from min. 8 on at $8000\,\mathrm{min^{-1}}$ with step wise decreasing load. Water coolant intake at $80\,°\mathrm{C}$.

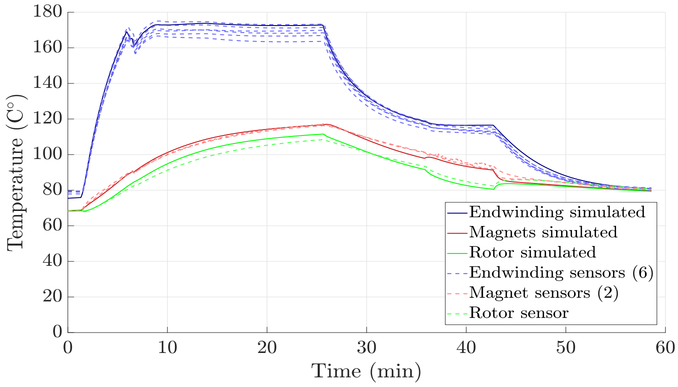

Fig. 8. High load at $4000\,\mathrm{min^{-1}}$, then $6000\,\mathrm{min^{-1}}$, then $9500\,\mathrm{min^{-1}}$. Water coolant intake at $80\,°\mathrm{C}$.

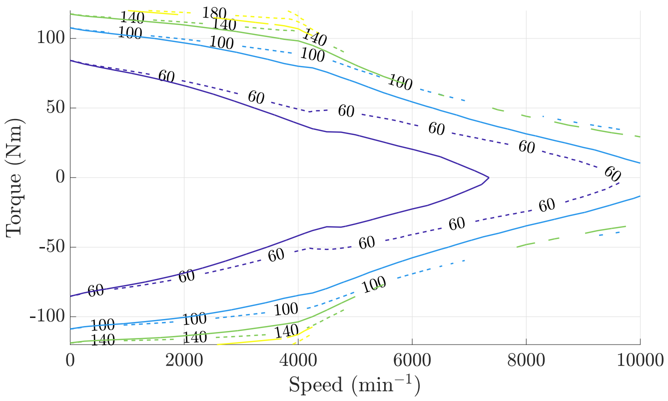

Fig. 9. Steady-state temperature of the permanent magnets with and without rotor cooling.

occurs at $10\,000\,\mathrm{min}^{-1}$ with more than $40\,\mathrm{K}$ difference to the non cooled rotor (see Fig. 9).

To illustrate impact of the temperature decrease the areas of possible continuous operation (S1) with and without rotor cooling (RC) have been calculated. Figure 10 shows that at $10\,000\,\mathrm{min}^{-1}$ the continuously possible torque or rather the power output rises by about $50\,\%$. Via simulation with a vehicle model of a common passenger car the continuous speed line was calculated below which a vehicle would decelerate. Also shown are the permitted magnet temperatures from the FEA simulation.

The rotor air cooling system significantly enlarges the area of continuous operation (S1 area) and therefor also the possible overload. It has to be mentioned that the water coolant intake temperature is the standardized $25\,°\mathrm{C}$ for determining the load capability of electrical machines. With a vehicle cooling system the coolant intake temperature is expected to be notably higher, reducing the heat removal through the water cooling jacket. This will further increase the effect of the rotor cooling.

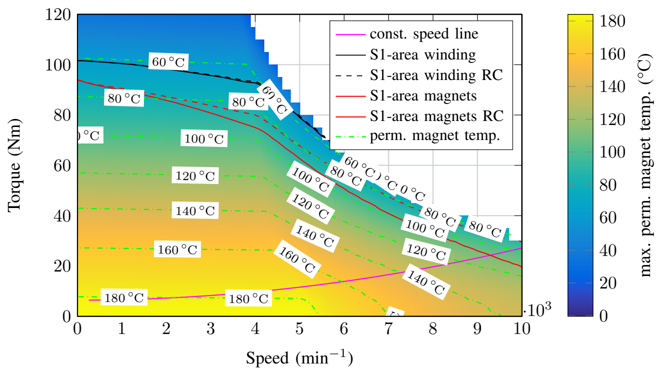

Fig. 10. Possible operation areas and permitted magnet temperatures. Coolant intake at $25\,°\mathrm{C}$.

VII. Conclusion

In this paper the effect of an air cooled rotor on the possible operation areas of a radial flux PMSM is investigated via thermal simulation. The rotor cooling yields a significant decrease in magnet temperature at high machine speed. This effectively enlarges the area of possible continuous operation as well as the possible overload. Due to the speed dependent cooling behavior the effect is largest at high machine speed which occurs at high vehicle speed where a high power output is required and cooling of the rotor is crucial. The results show a significant increase in thermal utilization of the motor.

VIII. Acknowledgement

The results presented in this paper have been developed in the research project e-MoSys: Entwicklung und prototypische Umsetzung eines anfordergungsgerechten und modularen Antriebs- und Fahrwerkssystems fr ein Elektrofahrzeug" granted by the Ministry of Education and Research (reference number 16N11637).

Federal Ministry of Education and Research

References

[1] A. S. Fawzal, R. M. Cirstea, K. N. Gyftakis, T. J. Woolmer, M. Dickison, M. Blundell, "Fan Performance Analysis for Rotor Cooling of Axial Flux Permanent Magnet Machines," *2016 22nd International Conference on Electrical Machines (ICEM)*, pp. 2725 - 2731, Nov. 2016.

[2] F.J. Marquez-Fernandez, J. H. J. Potgieter, A. G. Fraser, M. D. McCulloch, "Thermal management in a high speed switched reluctance machine for traction applications," *in 8th IET International Conference on Power Electronics, Machines and Drives (PEMD 2016)*, pp. 1-6, Nov. 2016.

[3] F. Marquez-Fernandez, A. Reinap, Z. Huang, M. Alkla, "Dynamic evaluation of the overloading potential of a convection cooled permanent magnet synchronous motor," *in IEEE International Electric Machines & Drives Conference (IEMDC)*, pp. 13-18, Aug. 2011.

[4] M. Hüske, M. Baydoun, A. Ruf, T. Plum, K. Hameyer and S. Pischinger, "Thermische Auslegung eines elektrischen Traktionsmotors unter Ausnutzung der Überlastfähigkeit," *in Haus der Technik Fachbuch*, Expert Verlag, pp. 195-215, 2015.

[5] VDI-Gesellschaft Verfahrenstechnik und Chemieingenieurswesen (GVC), *VDI-Wärmeatlas*, Springer-Verlag Berlin Heiderlberg, 2013.

[6] J. Pyrhönen, T. Jokinen and V. Hrabovcova, *Design of rotating electrical machines*, John Wilex & Sons Ltd., 2008.

[7] S. Steentjes, M. Lemann and K. Hameyer, "Advanced iron-loss calculation as a basis for efficiency improvement of electrical machines in automotive application," *in Electrical Systems for Aircraft, Railway and Ship Propulsion (ESARS)*, pp. 16, Oct. 2012.

[8] O. Wallscheid, "Design and empirical identification of a lumped parameter thermal network for permanent magnet synchronous motors with physically motivated constraints," *in 2015 IEEE International Electric Machines & Drives Conference (IEMDC)*, pp. 1380-1386, May 2015.

[9] T. Grosse, D. Franck, N. Conzelmann and K. Hameyer; D. Paul, C. Haenelt and A. Stapelmann, "Compact machine design of an integrated multiphase VPMSM," *in 2015 5th International Conference on Electric Drives Production (EDPC)*, pp.1-6, Nov. 2015.

[10] DIN EN 60085:2008-08 (IEC 60085:2007), Electrical insulation materials - Thermal endurance properties.